Catalysis Science & Technology

ROYAL SOCIETY OF CHEMISTRY

COMMUNICATION

View Article Online
View Journal | View Issue

Cite this: *Catal. Sci. Technol.*, 2021, 11, 6369

Received 5th August 2021,
Accepted 29th August 2021

DOI: 10.1039/d1cy01409a

rsc.li/catalysis

Potassium-incorporated manganese oxide enhances the activity and durability of platinum catalysts for low-temperature CO oxidation†

Xuelan Yan,[a] Tao Gan,[a] Shaozhen Shi,[a] Juan Du,[b] Guohao Xu,[a] Wenxiang Zhang,*[c] Wenfu Yan,[a] Yongcun Zou[a] and Gang Liu*[a]

Potassium ions in the tunnel of MnO_2 is demonstrated to significantly enhance the activity of surface oxygen species, which is favorable for preparing highly efficient Pt-based catalysts for low-temperature CO oxidation.

Catalytic CO oxidation has been attracting attention from the catalysis and materials science communities not only due to its role as a prototype reaction in heterogeneous catalysis but also due to its wide applications in numerous areas.[1–4] Any incomplete combustion of carbon-containing fuels and running of large equipment can produce harmful CO gas.[5,6] From the viewpoint of thermodynamics, CO oxidation is fairly easy due to the nature of exothermic downhill-type reactions.[7–10] The competitive activation of CO and O_2 over conventional catalysts could be balanced under relatively high temperatures.[11–13] The challenges of catalytic CO oxidation is under room temperature or lower. Under such conditions, O_2 dissociative adsorption govern the proceeding of the whole reaction.[14,15] Although significant progress has been made on the development of catalysts for room-temperature CO oxidation, simultaneously meeting the requirements of high activity and high stability in practical applications is still difficult.[16,17]

Pt-Based catalysts represent a kind of widely used emission control catalysts in industrial applications.[18–21] Most of these catalysts work under relatively high temperatures. The successful alternative Pt-based catalysts for room-temperature CO oxidation was realized through the introduction of ferrihydrite ($FeO(OH,H_2O)_n$) as a support, which was first reported by our group in 2008.[22] The ferrihydrite support directly participated in the O_2 activation, effectively lowering the barrier of O_2 dissociative adsorption.[23] Significant progresses have been made in the following years. However, the drawback of thermal instability of ferrihydrite and similar compounds still applies to this strategy.[24] The vulnerable nature of hydroxides and coordinately unsaturated sites significantly affects the activity of catalyst after long-term operation and storage.

Experiment evidences show that the participation of Fe-based compounds in O_2 activation is mainly dependent on surface hydroxides and Fe ions undergoing valence change between +2 and +3.[25] Except for the decrease in surface hydroxides under oxygen-rich or ambient conditions, Fe^{2+} ions would be irreversibly oxidized to Fe^{3+} ions, causing a decrease in activity.[26] In contrast, the multivalent nature of manganese (the most common oxidation states are +2, +3, and +4) endow the manganese oxide with intrinsic advantages for redox reactions.[27–30] Some positive effects have been observed from pristine or modified MnO_2 as oxidation catalysts.[31–35] In this regard, we think MnO_2 could be used as a suitable candidate to fabricate robust Pt-based catalysts for low temperature CO oxidation. The critical problem is to find what type of MnO_2 is more suitable for coupling Pt to complete active oxygen supplying and replenishing cycles at low temperatures.

Current research recognizes that the crystal structure significantly influences the catalytic oxidation activity of MnO_2, which determines the formation energy of oxygen vacancies.[36–38] A lower vacancy formation energy would correlate with a better molecular O_2 activation activity.[39,40] However, our present work demonstrated that this principle mainly applies to pristine MnO_2 catalysts in CO oxidation. When coupling with Pt nanoparticles, unexpected enhancement was observed based on K-incorporated MnO_2 as supports. Characterization results showed that the presence

[a] *State Key Laboratory of Inorganic Synthesis and Preparative Chemistry, College of Chemistry, Jilin University, Changchun, 130012, China. E-mail: lgang@jlu.edu.cn*
[b] *Key Laboratory of Preparation and Application of Environmental Friendly Materials (Jilin Normal University), Ministry of Education, Changchun, 130103, China*
[c] *Institute of Physical Chemistry, College of Chemistry, Jilin University, Changchun, 130012, China. E-mail: zhwenx@jlu.edu.cn*

† Electronic supplementary information (ESI) available: Experimental details and supporting characterization details such as XRD, TEM, HRTEM and BET. See DOI: 10.1039/d1cy01409a

of K in the tunnel of MnO_2 significantly improved the activity of surface oxygen species, resulting in the high performance of supported-Pt catalysts at low temperatures.

In our investigation, we first considered the formation energy of oxygen vacancy of MnO_2 to select suitable supports. The formation energy of oxygen vacancy is an important descriptor for the oxidizing capability of oxide-related catalysts. Taking into account the formation energy of oxygen vacancy previously reported by studies,[41] four crystallographic structures α-, β-, γ- and δ-MnO_2 were adopted. Fig. 1 shows the crystal structures of these MnO_2 substrates. Among them, hollandite-type α-MnO_2 and pyrolusite-type β-MnO_2 have one-dimensional (1 × 1) and (2 × 2) tunnel structures. Nsutite-type γ-MnO_2 is composed of an intergrowth of (1 × 1) tunnels (pyrolusite) and (1 × 2) tunnels (ramsdellite), while birnessite δ-MnO_2 has a layered structure.[42] The significant difference between δ-MnO_2 and other three crystal phase is that δ-MnO_2 contains intercalated K cations between the MnO_2 octahedral sheets. In our case, we denoted this sample as δ-MnO_2(K). For comparison, the α-MnO_2 sample with the incorporated K in the tunnels and loading on the surface of α-MnO_2 was also considered, which was denoted as α-MnO_2(K) and K/α-MnO_2.

All these MnO_2 samples were prepared by hydrothermal methods (see the ESI† for the details of synthesis). XRD patterns confirm the formation of corresponding structures, which are tetragonal α-MnO_2 (JCPDS 00-044-0141), tetragonal β-MnO_2 (JCPDS 00-024-0735), orthorhombic γ-MnO_2 (JCPDS 00-014-0644) and trigonal δ-MnO_2 (JCPDS 01-073-7867). In comparison with pristine α-MnO_2, a slight shift in the diffraction peak could be observed from the XRD pattern of α-MnO_2(K), which indicates the incorporation of K ions in the tunnels (Fig. S1†).[43] As for K/α-MnO_2, little change in XRD patterns can be observed (Fig. S1†). All these MnO_2 samples are active in CO oxidation at relatively high temperatures. They exhibit similar activity trends under both dry and moist conditions (Fig. 2a and b). Taking into account the energy value and the ratio of oxygen sites, theoretical

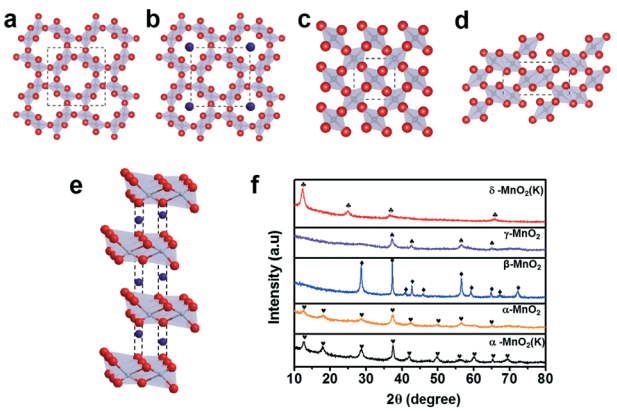

Fig. 1 Structures and XRD patterns of (a) α-MnO_2, (b) α-MnO_2(K), (c) β-MnO_2, (d) γ-MnO_2, (e) δ-MnO_2(K). Gray, purple, and red spheres represent Mn, K, and O atoms, respectively. (f) XRD patterns of MnO_2 with different crystal phases.

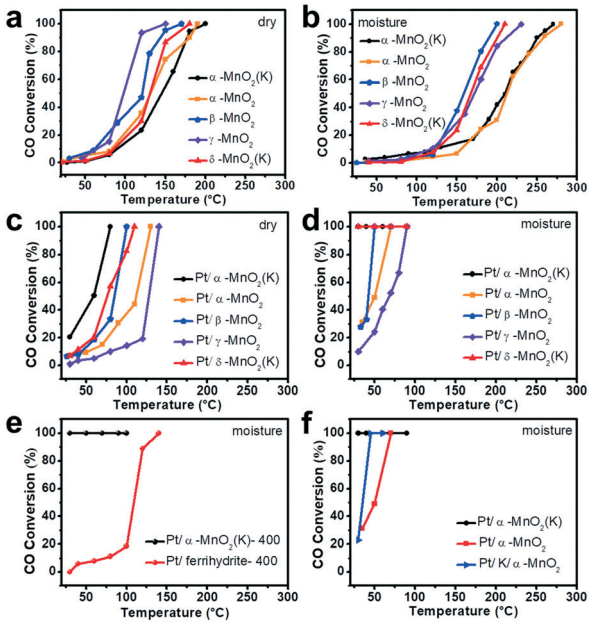

Fig. 2 Catalytic activities of CO oxidation over different catalysts. (a and b) MnO_2 supports with different structures. (c and d) Pt/MnO_2 catalysts with different crystal phases. (e) Pt/α-MnO_2(K)-400 and Pt/ferrihydrite-400 samples. (f) Pt/α-MnO_2(K), Pt/α-MnO_2 and Pt/K/α-MnO_2. Reaction conditions: (a and c) GHSV = 60 000 mL g^{-1} h^{-1}, 1 vol% CO, 5 vol% O_2/Ar and Ar balance. (b and d–f) GHSV = 60 000 mL g^{-1} h^{-1}, 1 vol% CO, 4 vol% H_2O, 5 vol% O_2/Ar and Ar balance.

calculation results reported by Hayashi *et al.* showed that β-MnO_2 and γ-MnO_2 have lower vacancy formation energies.[41] These two samples exhibit obvious advantages over α-MnO_2 as oxidation catalysts. Our experimental results on pristine MnO_2 are consistent with theoretical calculation results of vacancy formation energies. The incorporation of K ions in the tunnel of α-MnO_2 has little effect on the improvement of the catalytic performance of pristine MnO_2.

Significant changes were observed over MnO_2 supported-Pt catalysts. They exhibit a different activity trend from that of pristine MnO_2 (Fig. 2c and d). The catalysts were prepared by a colloidal deposition method similar to a method reported in our previous work on iron oxide-supported Pt catalysts[22] where Pt nanoparticles were pre-prepared by a polyol reduction route and highly dispersed on the surface of MnO_2 supports (Fig. S2 and S3†). Among them, Pt/α-MnO_2(K) and Pt/δ-MnO_2(K) exhibit evident higher activity than Pt/β-MnO_2 and Pt/γ-MnO_2 in CO oxidation. Moreover, both Pt/α-MnO_2(K) and Pt/δ-MnO_2(K) could realize the complete conversion of CO (SV = 60 000 mL g^{-1} h^{-1}) to CO_2 at room temperature in the presence of water gas (4 vol%). It is known that ferrihydrite ($FeO(OH,H_2O)_n$) as a support could effectively lower the barrier of Pt for CO oxidation. Pt/ferrihydrite was recognized as one of the state-of-art catalysts for low-temperature CO oxidation. The drawback is the intrinsic thermally unstable nature of hydroxides. It directly influences the duration of the catalyst under long-term work or storage. For meeting the requirement of potential

applications, in our case, a relatively harsh thermal treatment was carried out. After treating at 400 °C for 4 h, a significant decrease in activity can be observed over Pt/ferrihydrite-400 (Fig. 2e). In sharp contrast, Pt/α-MnO_2(K)-400 still maintained the high activity for room-temperature CO oxidation (Fig. 2e). No deactivation was observed in the whole test period (Fig. S4†). In addition, almost no change can be observed between fresh and used samples (Fig. S5†). All these enhancements of catalytic performance should be ascribed to the multivalent nature of Mn in manganese oxide.

However, different from our prediction, there is no direct relationship between the vacancy formation energies of MnO_2 and catalytic performance of supported-Pt catalysts. The high performance of Pt/α-MnO_2(K) and Pt/δ-MnO_2(K) might correlate with the incorporation of K ions in the tunnel of α-MnO_2 and δ-MnO_2. Such K ions originate from the precursor of $KMnO_4$. Inductively coupled plasma (ICP) measurements show that the amounts of K in Pt/α-MnO_2(K) and Pt/δ-MnO_2(K) are 2.87% and 2.90%, respectively. Trace amounts of K could be detected in other two phase MnO_2. For understanding the effects of K on the catalytic performance, a similar amount of K was loaded on the surface of α-MnO_2 by the impregnation method (denoted as K/α-MnO_2). The catalytic performance of the resultant Pt/K/α-MnO_2 is higher than that of Pt/α-MnO_2, and lower than that of Pt/α-MnO_2(K) (Fig. 2f). This result confirms the positive role of K ions in the enhancement of catalytic performance of the supported Pt catalysts.

It is well-known that alkali metal species can efficiently promote the performance of heterogeneous catalysis *via* multiple ways, such as modifying the active sites or influencing the adsorption behavior.[44–47] In a recent study, theoretical results reported by Hao *et al.* showed that K^+ in the tunnels of α-MnO_2 could form a stable coordination with eight nearby O_{sp3} atoms.[43] This interaction could rearrange the charge population of nearby Mn and O atoms, and finally make the topmost five-coordinated unsaturated Mn cations more positive. In our case, XPS is carried out to detect the chemical states of surface Mn and O species. Compared with Pt/α-MnO_2, the $Mn2p_{3/2}$ and $Mn2p_{1/2}$ peaks of Pt/α-MnO_2(K) shift to a relatively high binding energy (Fig. 3a). Moreover, the O1s peak of Pt/α-MnO_2(K) shifts to a low binding energy (Fig. 3b). Similar phenomena were also observed on the Pt/δ-MnO_2(K) sample (Fig. 3a and b). These results are consistent with the theoretical results on the rearrangement of the charge between Mn and O atoms. Remarkably, it directly influences the electronic properties of Pt nanoparticles and activities of surface oxygen species. Besides the O_2 activation, CO oxidation simultaneously includes the adsorption and activation of CO molecules. This process is easy to achieve over Pt nanoparticles, and should be difficult on pristine MnO_2. It should be the critical reason that the incorporation of K ions in the tunnels could increase the activity of supported Pt catalysts, while has little influence on pristine MnO_2.

Fig. 3c shows the Fourier-transform infrared (FTIR) spectroscopy of CO adsorption, and provides the information

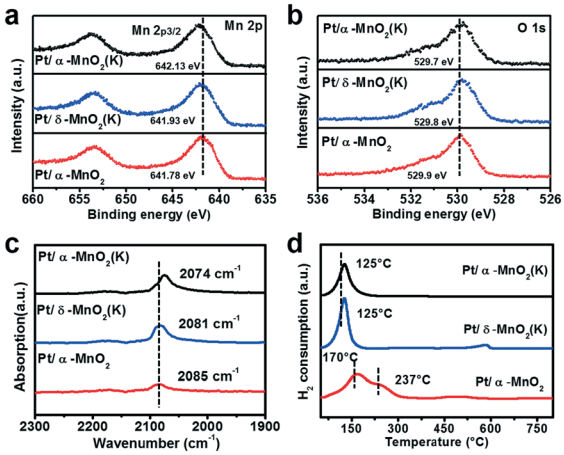

Fig. 3 Characterization of the surface properties of Pt/α-MnO_2(K), Pt/δ-MnO_2(K) and Pt/α-MnO_2. (a and b) Mn 2p, O 1s XPS spectra (c) typical FTIR spectra collected exposure to the CO. (d) H_2-TPR profiles.

about the oxidation state of Pt. The bands at about 2080 cm^{-1} are ascribed to the linearly bonded CO on Pt^0 sites.[48] The redshift of this band over Pt/α-MnO_2(K) and Pt/δ-MnO_2(K) indicates much more charge transfer from the MnO_2 support to Pt centers. Moreover, a sharp H_2 consumption peak at 125 °C can be observed in the H_2-TPR spectra of Pt/α-MnO_2(K) and Pt/δ-MnO_2(K). As for Pt/α-MnO_2, this peak is relatively broad and shift to higher temperatures. These reducible properties indicate that the surface oxygen species of Pt/α-MnO_2(K) and Pt/δ-MnO_2(K) are more active than those of Pt/α-MnO_2.

In our case, the high activity of Pt/α-MnO_2(K) and Pt/δ-MnO_2(K) should correlate with the unique electronic properties of Pt nanoparticles and active surface oxygen species. We carried out *in situ* DRIFT to investigate the CO

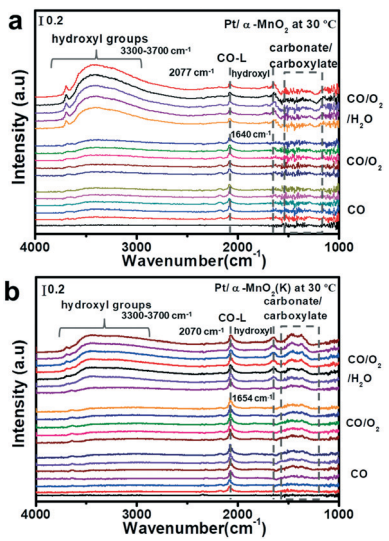

Fig. 4 *In situ* DRIFT spectra of CO oxidation over Pt/α-MnO_2(K) and Pt/α-MnO_2 catalysts under reaction conditions at 30 °C: (a) Pt/α-MnO_2; (b) Pt/α-MnO_2(K).

oxidation over Pt/α-MnO_2 and Pt/α-MnO_2(K) at different temperatures. In comparison with Pt/α-MnO_2 (Fig. 4a and S6a†), carbonate species (1200–1600 cm^{-1}) can be observed clearly over Pt/α-MnO_2(K) (Fig. 4b and S6b†) when introducing CO into the reaction cell.[49] This result indicates that CO could react with the surface oxygen species α-MnO_2(K). When further introducing O_2 into the cell, the adsorbed CO could be conversed completely over Pt/α-MnO_2(K) at 100 °C (Fig. S6b†). At 30 °C, such conversion of CO cannot proceed smoothly. It needs the participation of hydroxide origin from H_2O. Density functional theory calculations based on CeO_2 catalysts discloses a new pathway for CO oxidation,[50] in which carbonate intermediates formed during reaction exhibit active property and could react with CO to form CO_2. In comparison with directly dissociating carbonate, the reaction between carbonate and CO is with much lower energy barrier. According to DRIFT and catalytic tests, it can be speculated that CO oxidation over Pt/α-MnO_2(K) should obey the carbonate-mediated Mars van Krevelen mechanism. The presence of K in the tunnel of MnO_2 significantly improves the activity of surface oxygen species, resulting in the high performance of supported-Pt catalysts at low temperatures.

In summary, systematic investigation shows that the presence of K ions in the tunnel of MnO_2 could significantly improve the activity of surface oxygen species. By coupling Pt nanoparticles, MnO_2 could serve as supports to fabricate highly efficient catalysts for low-temperature CO oxidation. Such catalysts exhibit relatively high thermal stability in comparison with ferrihydrite-based catalysts. This work would open an alternative way to prepare highly active Pt-based catalysts for catalytic oxidation.

This work was supported by the National Science Foundation of China (22072054 and 21972053), the Development Project of Science and Technology of Jilin Province (20170101171JC and 20180201068SF), the Open Project of State Key Laboratory of Inorganic Synthesis and Preparative Chemistry (202105) and the Open Project Program of Key Laboratory of Preparation and Application of Environmental Friendly Materials (Jilin Normal University), Ministry of Education, China (No. 2020009).

Conflicts of interest

There are no conflicts to declare.

Notes and references

1 Y. Li, L. Lin, R. Mu, Y. Liu, R. Zhang, C. Wang, Y. Ning, Q. Fu and X. Bao, *ACS Catal.*, 2021, **11**, 849–857.
2 H. J. Freund, G. Meijer, M. Scheffler, R. Schlogl and M. Wolf, *Angew. Chem., Int. Ed.*, 2011, **50**, 10064–10094.
3 S. Liu, W. Xu, Y. Niu, B. Zhang, L. Zheng, W. Liu, L. Li and J. Wang, *Nat. Commun.*, 2019, **10**, 5790.
4 T. Wang, J. Y. Xing, A. P. Jia, C. Tang, Y. J. Wang, M. F. Luo and J. Q. Lu, *J. Catal.*, 2020, **382**, 192–203.
5 L. Wang, S. Deo, K. Dooley, M. J. Janik and R. M. Rioux, *Chin. J. Catal.*, 2020, **41**, 951–962.
6 H. Guan, Y. Chen, C. Ruan, J. Lin, Y. Su, X. Wang and L. Qu, *Chin. J. Catal.*, 2020, **41**, 613–621.
7 X. Liu, M. Xu, L. Wan, H. Zhu, K. Yao, R. Linguerri, G. Chambaud, Y. Han and C. Meng, *ACS Catal.*, 2020, **10**, 3084–3093.
8 H. Falsig, B. Hvolbaek, I. S. Kristensen, T. Jiang, T. Bligaard, C. H. Christensen and J. K. Norskov, *Angew. Chem., Int. Ed.*, 2008, **47**, 4835–4839.
9 M. Kim, M. Bertram, M. Pollmann, A. von Oertzen, A. S. Mikhailov, H. H. Rotermund and G. Ertl, *Science*, 2001, **292**, 1357–1360.
10 C. Chi, H. Qu, L. Meng, F. Kong, M. Luo and M. Zhou, *Angew. Chem., Int. Ed.*, 2017, **56**, 14096–14101.
11 I. Ro, I. B. Aragao, J. P. Chada, Y. Liu, K. R. Rivera-Dones, M. R. Ball, D. Zanchet, J. A. Dumesic and G. W. Huber, *J. Catal.*, 2018, **358**, 19–26.
12 S. Song, Y. Wu, S. Ge, L. Wang, Y. Wang, Y. Guo, W. Zhan and Y. Guo, *ACS Catal.*, 2019, **9**, 6177–6187.
13 M. J. Kale and P. Christopher, *ACS Catal.*, 2016, **6**, 5599–5609.
14 I. X. Green, W. J. Tang, M. Neurock and J. T. Yates, *Science*, 2011, **333**, 736–739.
15 I. X. Green, W. Tang, M. McEntee, M. Neurock and J. T. Yates, *J. Am. Chem. Soc.*, 2012, **134**, 12717–12723.
16 B. Zheng, T. Gan, S. Shi, J. Wang, W. Zhang, X. Zhou, Y. Zou, W. Yan and G. Liu, *ACS Appl. Mater. Interfaces*, 2021, **13**, 27029–27040.
17 B. Zheng, S. Wu, X. Yang, M. Jia, W. Zhang and G. Liu, *ACS Appl. Mater. Interfaces*, 2016, **8**, 26683–26689.
18 A. K. Datye and M. Votsmeier, *Nat. Mater.*, 2021, **20**, 1049–1059.
19 J. Jones, H. F. Xiong, A. T. Delariva, E. J. Peterson, H. Pham, S. R. Challa, G. S. Qi, S. Oh, M. H. Wiebenga, X. I. P. Hernandez, Y. Wang and A. K. Datye, *Science*, 2016, **353**, 150–154.
20 B. Qiao, A. Wang, X. Yang, L. F. Allard, Z. Jiang, Y. Cui, J. Liu, J. Li and T. Zhang, *Nat. Chem.*, 2011, **3**, 634–641.
21 A. Beniya and S. Higashi, *Nat. Catal.*, 2019, **2**, 590–602.
22 S. Li, G. Liu, H. Lian, M. Jia, G. Zhao, D. Jiang and W. Zhang, *Catal. Commun.*, 2008, **9**, 1045–1049.
23 L. Liu, F. Zhou, L. Wang, X. Qi, F. Shi and Y. Deng, *J. Catal.*, 2010, **274**, 1–10.
24 B. Zheng, G. Liu, L. Geng, J. Cui, S. Wu, P. Wu, M. Jia, W. Yan and W. Zhang, *Catal. Sci. Technol.*, 2016, **6**, 1546–1554.
25 G. X. Chen, Y. Zhao, G. Fu, P. N. Duchesne, L. Gu, Y. P. Zheng, X. F. Weng, M. S. Chen, P. Zhang, C. W. Pao, J. F. Lee and N. F. Zheng, *Science*, 2014, **344**, 495–499.
26 L. Cao, W. Liu, Q. Luo, R. Yin, B. Wang, J. Weissenrieder, M. Soldemo, H. Yan, Y. Lin, Z. Sun, C. Ma, W. Zhang, S. Chen, H. Wang, Q. Guan, T. Yao, S. Wei, J. Yang and J. Lu, *Nature*, 2019, **565**, 631–635.
27 I. Kruk, P. Zajdel, W. van Beek, I. Bakaimi, A. Lappas, C. Stock and M. A. Green, *J. Am. Chem. Soc.*, 2011, **133**, 13950–13956.

28 J. Hou, Y. Li, M. Mao, Y. Yue, G. N. Greaves and X. Zhao, *Nanoscale*, 2015, **7**, 2633–2640.
29 X. Yu, J. He, D. Wang, Y. Hu, H. Tian and Z. He, *J. Phys. Chem. C*, 2011, **116**, 851–860.
30 J. C. Villegas, L. J. Garces, S. Gomez, J. P. Durand and S. L. Suib, *Chem. Mater.*, 2005, **12**, 1910–1918.
31 N. Jain and A. Roy, *Mater. Res. Bull.*, 2020, **121**, 110615.
32 N. Zhang, L. Li, R. Wu, L. Song, L. Zheng, G. Zhang and H. He, *Catal. Sci. Technol.*, 2019, **9**, 347–354.
33 J. Gao, C. Jia, L. Zhang, H. Wang, Y. Yang, S.-F. Hung, Y.-Y. Hsu and B. Liu, *J. Catal.*, 2016, **341**, 82–90.
34 J. Zhang, Y. Li, L. Wang, C. Zhang and H. He, *Catal. Sci. Technol.*, 2015, **5**, 2305–2313.
35 K. Li, J. Chen, Y. Peng, W. Lin, T. Yan and J. Li, *J. Mater. Chem. A*, 2017, **5**, 20911–20921.
36 E. W. McFarland and H. Metiu, *Chem. Rev.*, 2013, **113**, 4391–4427.
37 L. Li, X. Feng, Y. Nie, S. Chen, F. Shi, K. Xiong, W. Ding, X. Qi, J. Hu, Z. Wei, L.-J. Wan and M. Xia, *ACS Catal.*, 2015, **5**, 4825–4832.
38 D. A. Tompsett, S. C. Parker and M. S. Islam, *J. Am. Chem. Soc.*, 2014, **136**, 1418–1426.
39 V. Agarwal and H. Metiu, *J. Phys. Chem. C*, 2016, **120**, 2320–2323.
40 K. Kamata, K. Sugahara, Y. Kato, S. Muratsugu, Y. Kumagai, F. Oba and M. Hara, *ACS Appl. Mater. Interfaces*, 2018, **10**, 23792–23801.
41 E. Hayashi, Y. Yamaguchi, K. Kamata, N. Tsunoda, Y. Kumagai, F. Oba and M. Hara, *J. Am. Chem. Soc.*, 2019, **141**, 890–900.
42 R. Yang, Y. Fan, R. Ye, Y. Tang, X. Cao, Z. Yin and Z. Zeng, *Adv. Mater.*, 2021, **33**, e2004862.
43 Z. Hao, Z. Shen, Y. Li, H. Wang, L. Zheng, R. Wang, G. Liu and S. Zhan, *Angew. Chem., Int. Ed.*, 2019, **58**, 6351–6356.
44 P. Panagiotopoulou and D. I. Kondarides, *J. Catal.*, 2009, **267**, 57–66.
45 C. Stoffelsma, P. Rodriguez, G. Garcia, N. Garcia-Araez, D. Strmcnik, N. M. Markovic and M. T. M. Koper, *J. Am. Chem. Soc.*, 2010, **132**, 16127–16133.
46 Y. Zhai, D. Pierre, R. Si, W. Deng, P. Ferrin, A. U. Nilekar, G. Peng, J. A. Herron, D. C. Bell, H. Saltsburg, M. Mavrikakis and M. Flytzani-Stephanopoulos, *Science*, 2010, **329**, 1633–1636.
47 M. Yang, S. Li, Y. Wang, J. A. Herron, Y. Xu, L. F. Allard, S. Lee, J. Huang, M. Mavrikakis and M. Flytzani-Stephanopoulos, *Science*, 2014, **346**, 1498–1501.
48 M. J. Kappers and J. H. van der Maas, *Catal. Lett.*, 1991, 365–374.
49 K. Ament, N. Kowitsch, D. Hou, T. Gotsch, J. Krohnert, C. J. Heard, A. Trunschke, T. Lunkenbein, M. Armbruster and J. Breu, *Angew. Chem., Int. Ed.*, 2021, **60**, 5890–5897.
50 B. Liu, W. Li, W. Song and J. Liu, *Phys. Chem. Chem. Phys.*, 2018, **20**, 16045–16059.